Journal of Physics: Conference Series **484** (2014) 012041 doi:10.1088/1742-6596/484/1/012041

The CFHTLS-Strong Lensing Legacy Survey (SL2S): Investigating the group-scale lenses with the SARCS sample

A More[1,2*], R Cabanac[3,4], S More[1], C Alard[5], M Limousin[2], J-P Kneib[2], R Gavazzi[5] and V Motta[6]

[1] Kavli Institute for Cosmological Physics, University of Chicago, 5640 S. Ellis Ave., Chicago IL-60637, USA
[2] Laboratoire d'Astrophysique de Marseille, 38 rue Frederic Joddress 13013 Marseille, France
[3] Université de Toulouse, UPS-OMP, IRAP, Tarbes, France
[4] CNRS, IRAP, 57, Ave. d'Azereix, 65000 Tarbes, France
[5] Institute d'Astrophysique de Paris, France
[6] Universidad de Valparaiso, Departamento de Fisica y Astronomia, Avenida Gran Bretana 1111, Valparaiso, Chile

E-mail: *anupreeta@kicp.uchicago.edu

Abstract. We have presented the Strong Lensing Legacy Survey - ARCS (SARCS) sample compiled from the T0006 data release of the Canada-France-Hawaii Telescope Legacy Survey (CFHTLS) covering a total non-overlapping area of 159 deg^2. We have adopted a semi-automatic method to find gravitational arcs in the survey that makes use of an arc-finding algorithm. The SARCS sample consists of 127 lens candidates, out of which, 54 systems are promising lenses. From our sample, we have detected a systematic alignment of the giant arcs with the major axis of the baryonic component of the putative lens in concordance with previous studies. This alignment is also observed for all arcs in the sample and does not vary significantly with increasing arc radius. Owing to the large area and depth of the CFHTLS, we have found the largest sample of lenses probing mass scales that are intermediate to cluster and galaxy lenses for the first time. We have compared the observed image separation distribution (ISD) of our arcs with theoretical models. A two-component density profile for the lenses, which accounts for both the central galaxy and the dark matter component is required by the data to explain the observed ISD. Unfortunately, current levels of uncertainties and degeneracies accommodate models both with and without adiabatic contraction. We have also shown the effects of changing parameters of the model that predict the ISD and that a larger lens sample might constrain relations such as the concentration-mass relation, mass-luminosity relation and the faint-end slope of the luminosity function.

1. Introduction

Gravitational lensing is the deflection of light coming from distant sources in the Universe, due to the gravitational potential of intervening structures [1, 2]. The last decade has seen the rise of a wide variety of applications of strong lensing such as the study of distant lensed galaxies with unprecedented magnification [3, 4], the constraints on sub-structure within lensing halos [5, 6], accurate measurements of the Hubble constant [7], constraints on the stellar initial mass function [8], and constraints on the slope of the inner density profile of the lensing halos

[9, 10, 11]. Although strong lensing is a rare event, several surveys covering a wide sky area and deep enough imaging across different wavelengths, have resulted in the discovery of over 200 strong lens systems at galaxy scales from surveys such as the Cosmic Lens All Sky Survey [12], the Sloan Lens ACS Survey [13], and about a few dozen lens systems at cluster scales such as, the Extended Medium Sensitivity Survey [14], the MAssive Cluster Survey (MACS) [15], the Las Campanas Distant Cluster Survey [16], and the Red sequence Cluster Survey [17].

Majority of the surveys in the past have primarily focused on studying galaxy-scale or cluster-scale structures. As a result, matter distribution in galaxies and galaxy clusters is relatively well-studied via both strong and weak lensing. A further improvement in our understanding has come from the use of complementary methods to lensing such as stellar kinematics, satellite kinematics and X-ray scaling relations. In contrast, little is known about galaxy groups which are intermediate to galaxies and galaxy clusters, typically corresponding to masses of $10^{12}-10^{14}\ M_{\odot}$. Relatively fewer investigations have been carried out with galaxy groups e.g., study of mass-to-light ratios with the Canadian Network for Observational Cosmology 2 sample [18], study of faint end of the luminosity function of nearby compact groups [19], study of concentration-mass (c-M) relation from the SDSS [20] via weak lensing, study of colours and star formation [21], and study of scaling relations of X-ray selected groups [22]. Since studies of groups are limited, and we still do not have a detailed understanding of matter distribution, formation and evolution of galaxy groups. Being one of the important components in the hierarchical assembly of structures in the Universe, galaxy groups are much more massive than galaxy-scale halos and are concentrated enough to act as lenses. Furthermore, since galaxy groups are quite abundant compared to massive structures like galaxy clusters, the probability to find group scale lenses is also large. Hence, lensing can be successfully used to study group-scale halos.

The Strong Lensing Legacy Survey (SL2S) [23] is a survey from the Canada-France-Hawaii Telescope Legacy Survey (CFHTLS). The design of the CFHTLS allows us to find large sample of group-scale lenses, which can be studied in detail upto high redshifts, for the first time. The SL2S is as a precursor to wide field imaging surveys such as the Dark Energy Survey, Large Synoptic Survey Telescope and Euclid. In this paper, we have presented the SL2S-ARCS sample from the final T0006 release of the CFHTLS. In Section 2, we have given an overview of the survey and procedure of sample selection and present the final sample. In Section 3, we have discussed some statistical results using the final sample, and in Section 4, we have summarized the survey and our main findings.

2. The CFHTLS-SL2S ARCS sample

In this section, we have given a brief overview of the survey from which we have derived the lens sample.

2.1. Survey overview

CFHTLS is a photometric survey made with the Canada-France-Hawaii Telescope (CFHT) in five optical bands ($u^*g'r'i'z'$) using the wide-field imager MegaPrime with a field-of-view of 1 deg^2 on the sky and a pixel size of $0.186''$. The WIDE and DEEP components of the CFHTLS are designed to carry out extragalactic research. These components are ideal for searching strong lens systems. The SL2S sample is compiled from the CFHTLS-WIDE encompassing a combined area of 171 deg^2 and CFHTLS-DEEP encompassing a combined area of 4 deg^2. However, taking into account the masked and overlapping areas, the effective area of the survey is 150.4 deg^2 (146.9 deg^2 for WIDE and 3.5 deg^2 for DEEP). The WIDE and DEEP each consist of four fields[1]. Each of the deep fields covers an area of 1 deg^2. Among the WIDE fields,

[1] These numbers are estimated from
[http://terapix.iap.fr/cplt/table_syn_T0006.html] [http://terapix.iap.fr/cplt/table_syn_T0006.html]

g band imaging is the deepest of all bands with a limiting magnitude of 25.47 and a mean seeing of $0.78''$ whereas the g band imaging of DEEP fields has nearly 10 times deeper exposures than the WIDE fields, and the median seeing is $\sim 0.7''$. Further details of the T0006 release, which is the first complete release of the WIDE and DEEP, can be found on Terapix website[2].

2.2. Sample selection and output

We have defined the SARCS sample such that lens systems with arc radius ($R_{\rm A}$) $\geq 2''$ belong to the sample. The radius of the arc is defined as the distance of the lensed image from the putative lens galaxy which is roughly the Einstein radius. Typically, lensing halos with Einstein radius larger than $2''$ are very massive lenses with significant contribution from the environment of the primary lensing galaxy. Thus, the SARCS sample, predominantly, consists of group to cluster scale lenses.

The SARCS sample from the CFHTLS is compiled in a three-step process: (i) Run the arc-detection algorithm called ARCFINDER [24]. We have chosen to run the ARCFINDER on the g-band image since most of the lensed images correspond to galaxies with high star formation that have little emission at redder wavelengths. At the end of the first step, we have produced a list of arc candidates with various parameters. (ii) Apply a cut-off on arc properties such as the area, the peak flux count, the radius of curvature, and reject candidates within masked area. These cuts allow a significant reduction in false detections at the cost of losing some real arc candidates. (iii) Visual inspection, and classification are carried out to grade the quality of the candidates. Note that the final SARCS sample consists of candidates that are detected by the ARCFINDER and/or by visual inspection.

After the automatic detection and screening, about 1000 candidates/deg^2 are visually inspected. This is reduced to a total sample of 413 candidates, which is further considered for ranking by three people. Finally, we have accepted 127 lens candidates in the SARCS sample[3], which are ranked 2 or higher (average of the ranks by three people), and have $R_A > 2''$.

3. Results and discussion

In the following subsections, we have described the main findings from the SARCS sample and constraints on average properties of the lens population using statistical properties of the arcs.

3.1. Galaxy-arcs orientation

Triaxial dark matter halos, which appear elliptical in projection, may form lip caustics and giant arcs (high length-to-width ratio) are likely to occur in such cases (e.g., [25]). Using numerical simulations, authors of [26] have shown that the giant arcs are oriented very close to the major axis of the dark matter halo. If a central galaxy is further added to the halo, then it appeared to isotropize the angular distribution of arcs to a small extent. They have measured the angular distribution of giant arcs from the EMSS cluster sample, and found that most of the giant arcs had an orientation of < 45 deg, consistent with their predictions.

We have used the same definition as that of [26], that is, the angle between the major axis of the lens galaxy and the line connecting the centre of the lens galaxy to the midpoint of the arc. The midpoint of the arc and its orientation from the major axis of the lens is calculated manually. When there is a single dominant lensing galaxy, we have measured the position angle (PA) of the major axis of the lens galaxy with SEXTRACTOR [27], otherwise we have adopted the following strategy: If there are two or three (nearly collinear) lens galaxies with similar colours and brightness, then the PA of the ellipticity is assumed to be along the line joining the

[2] [http://terapix.iap.fr/cplt/T0006-doc.pdf] [http://terapix.iap.fr/cplt/T0006-doc.pdf]

[3] High resolution images of these systems are made available at http://kicp.uchicago.edu/∼anupreeta/sarcs sample.

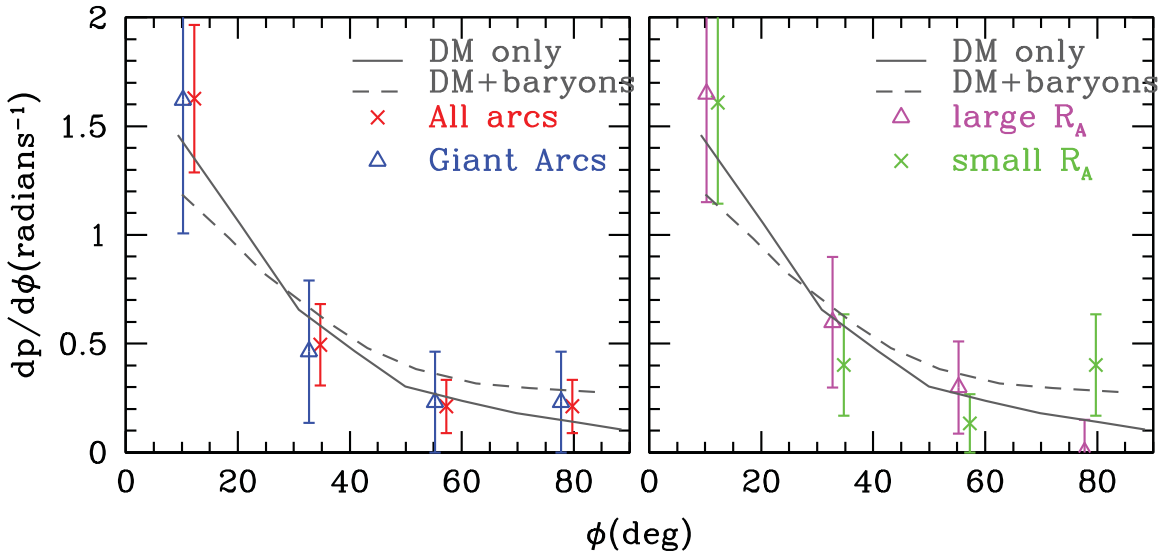

Figure 1. *Left*: Angular distribution of arcs with respect to the lens galaxy. The data points are from the SARCS sample. *Right*: The "all arcs" sample is divided into small and large $R_{\rm A}$. The expected curves for dark matter (DM) only (solid) and DM+$3 \times 10^{12} h^{-1} M_{\odot}$ (dashed) are taken from [26].

lens galaxies. If a circle going through the arc encloses multiple lens galaxies with comparable brightness but no obvious elongation, then such system is rejected.

After applying the above selection cuts, we are left with 36 all arc candidates and 11 giant arcs ($l/w \geq 8$) with an average ranking > 2.5. The angular distribution of the giant arcs from the SARCS sample is shown in the left panel of Figure 1. Our measurements are compared with predictions from [26], namely, (a) for dark matter only lensing halo (solid curve), and (b) a dark matter halo to which a galaxy of $3 \times 10^{12} h^{-1} M_{\odot}$ is added (dashed curve). The distribution of giant arcs from our sample appears to follow the expected trend although it is not possible to distinguish between the two curves. We have also found that the distribution of orientation of all arc candidates (see Figure 1) is consistent with expectations. This extends the result obtained in [26] to groups-scale lens systems.

We have further split the all arcs sample into a small $R_{\rm A}$ ($< 5''$) and large $R_{\rm A}$ ($\geq 5''$) samples to see the dependence of the angular distribution on the $R_{\rm A}$ with an arbitrary dividing value of $5''$. The baryonic matter tends to make the matter distribution in halos more spherical at the centre. Therefore, the angular distribution of arcs for the sample with smaller $R_{\rm A}$ is expected to be more isotropic compared to the sample with large $R_{\rm A}$. However, we do not find any clear differences in the angular distribution of small and large $R_{\rm A}$ for the SARCS sample within the uncertainties (see the right panel of Figure 1). We have noticed that these measurements may have some systematic errors due to the orientation dependence of the selection function. Ambiguities also exist in the definition of the orientation in few cases, especially when multiple candidate lens galaxies are involved. In addition, the current analysis consists of lens candidates as opposed to confirmed lens systems. Therefore, our conclusions should be treated more of a qualitative nature.

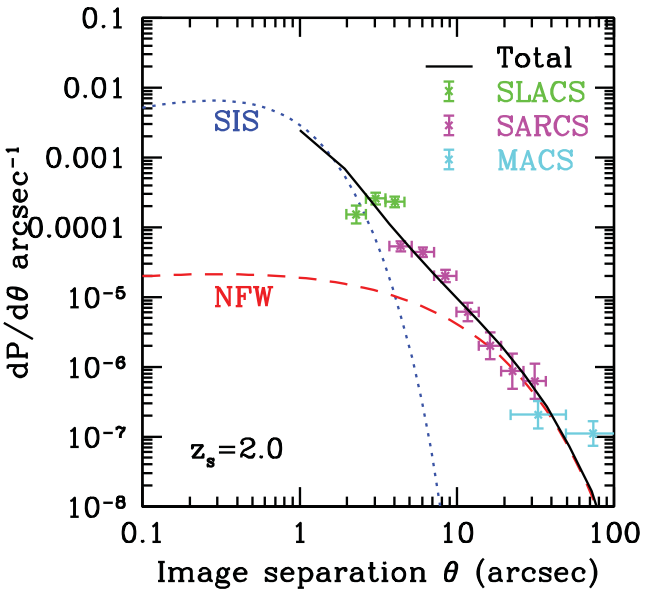

Figure 2. Image separation distribution. Theoretically calculated image separation distribution curves for SIS profile (dotted), NFW profile (dashed), and total profile (solid) following the model in [28]. The data points from the SARCS sample (magenta).

3.2. Image separation distribution

The image separation distribution (ISD) is sensitive to the halo mass, abundance of the lens population, the mass distribution in the lens, and the source redshift. Therefore, the ISD measured from galaxy to cluster scales contains information about the cosmological parameters and various scaling relations between galaxy properties and halo mass. Hitherto, the ISD has been measured either at small image separations (θ) primarily, with lens samples such as CASTLES (e.g., [29]) and CLASS (e.g., [28]) or at large θ with cluster-scale lenses, for example, the MACS sample [30]. With the SARCS sample, we can probe the intermediate mass regime corresponding to group scale lenses.

3.2.1. Model for the expected distribution: We have followed the framework developed in [28] to calculate the expected ISD in order to compare it with the observed ISD from the SARCS sample, and also adopted the cosmology, that is, $\Omega_m = 0.3$, $\Omega_\Lambda = 0.7$, and $\sigma_8 = 0.9$. The probability for a source at redshift z_s to get lensed with image separation greater than θ is $P(>\theta; z_s)$. The differential probability is then given by:

$$\left|\frac{\mathrm{d}P}{\mathrm{d}\theta}\right| = \int_0^{z_s} \mathrm{d}z_l \, \frac{\mathrm{d}\chi}{\mathrm{d}z_l} \, n(\tilde{M}[\theta], z_l) \, \sigma_{\rm lens} \Theta(M - \tilde{M}) \,, \qquad (1)$$

which can be directly related to the ISD of the observed lens sample. Here, χ is the comoving distance and z_l is the redshift of the lens, M corresponds to the halo mass, $n(M, z_l)$ is the halo mass function, $\tilde{M}$ is the minimum halo mass that causes an image separation equal to θ, and Θ is the Heaviside step function. The biased lensing cross section, $\sigma_{\rm lens}$ is measured in comoving units and includes $B(z_s)$, the magnification bias which causes sources, fainter than the limiting magnitude of the survey, to be detected in the sample.

In [28], the Eq. (1) is used to predict the ISD resulting from different components in a given halo. For the mass distribution inside a halo, the author in [28] has considered three types of density profiles: (i) isothermal (SIS) density profile, which is found to fit well galaxy-scale halos, (ii) NFW density profile, which is a good fit for dark matter halos in simulations and also in the observations of clusters, and (iii) A more complex "Total" profile, consisting of Hernquist [31] profile for the stellar distribution in the central regions and NFW profile for the underlying dark matter distribution along with adiabatic contraction model [32]. The author of [28] has assumed

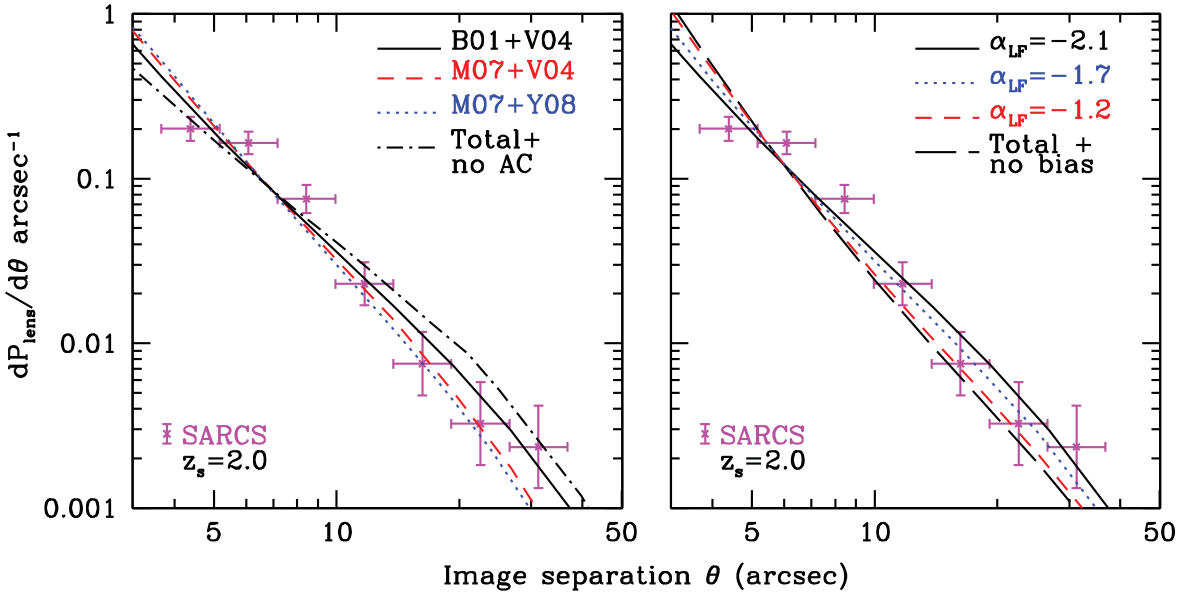

Figure 3. Image separation distribution. Theoretical curves for the total profile, shown with solid black line, are the same as in Figure 2. *Left:* Adopting the $c-M$ relation of [33] (dashed) steepens the ISD. The dotted curve, with $M-L$ relation of [35] and $c-M$ relation of [33], steepens it further but negligibly. The ISD without the AC model (dashed-dotted) is also shown. *Right:* The effect of varying slope of the source luminosity function on the ISD is shown for the total profile. The total profile without any magnification bias (long dashed) is independent of $\alpha_{\rm LF}$. Changes in various model parameters have degenerate effects on the expected ISD.

the background source population to lie at a redshift of $z_s = 2$, and the source luminosity function $\Phi(z_s, L) \propto L^{-2.1}$ appropriate for the radio survey CLASS [12][4]. We are able to reproduce the expected ISDs from [28], given by Eq. (1), for all the three density distributions mentioned above. The expected ISDs corresponding to these three density distributions are shown in Figure 2.

3.2.2. Observed distribution: The observed ISD is calculated by logarithmically binning the image separations of 125 SARCS candidates with $\theta_{\rm cut} \geq 20$ pixels (that is, $> 3.7''$) and an average ranking of 2 and above. The image separation for each lens candidate is taken as twice the Einstein radius or roughly the arc radius, which is the distance between the candidate lensed image and the centre of respective lens galaxy. Let $\theta - d\theta = \theta_{\rm l}$ and $\theta + d\theta = \theta_{\rm h}$, then the observed ISD is given by:

$$\left|\frac{dP_{\rm lens}}{d\theta}\right|_{\rm obs} = \frac{N(>\theta_{\rm h}) - N(>\theta_{\rm l})}{N(>\theta_{\rm cut}) 2d\theta}, \qquad (2)$$

where the total number of observed lenses is $N(>\theta_{\rm cut})$. The SARCS data points demonstrate that the average density profile of the halos, giving rise to the intermediate θ values ($\sim 3''-12''$), is best represented by a combined profile for the main galaxy, and the dark matter halo as opposed to a pure SIS or pure NFW profile. The vertical error-bars are calculated assuming Poisson number statistics and the horizontal bars show the bin width. We have noticed that effects due to purity or incompleteness of the SARCS sample are not accounted for in this plot.

[4] The luminosity density for such a steep faint end slope ($\alpha_{\rm LF} < -2$) diverges as $L \to 0$, and necessarily requires a cutoff below some value of $L_{\rm min}$.

3.2.3. Tests with varying models: Here, we have tested the effects of varying the different components of the model in [28], and compared against the observed ISD. First, we have tested the influence of excluding the AC while computing the total profile. This has the effect of making the expected ISD shallower as shown by the dashed-dotted curve in the left panel of Figure 3. Prima facie, the AC model fits the data better than the model without AC. However, as we have shown below, there are other degeneracies in the model which prevent us from ruling out the "no AC" model at high significance. Next, we have tested the effect of using different $c-M$ relations on the ISD. For example, we have used the $c-M$ relation by [33] instead of that given by [34]. The $c-M$ relation of [33] is roughly $15-20\%$ lower than that of [34]. The combined profile using the $c-M$ relation of [33] is shown by the dashed curve in the left panel of Figure 3. Within the current statistical limits on the data, both the $c-M$ relations appear plausible, although the data appears to slightly favour the $c-M$ relation of [33]. We have also tested the effect of using a more recent determination of the $M-L$ relation obtained by [35] from a sample of SDSS groups along with the $c-M$ relation of [33] for the combined total profile. The $M-L$ relation of [35] differ by $\sim$ 0.2 dex from that of [36] at the intermediate mass regime which is the regime of interest. This appears to cause a very negligible change in the predicted ISD.

We have tried to quantify the effect of varying the slope ($\alpha_{\rm LF}$) of the source luminosity function ($\Phi(L) \propto L^{\alpha_{\rm LF}}$) at the faint-end. This influences the lens cross-section via the magnification bias. The solid curve in Figure 3 shows the expected ISD using the fiducial value of $\alpha_{\rm LF}=-2.1$, while the dotted and short dashed curves show the ISD in the right panel, corresponding to $\alpha_{\rm LF}$ equal to -1.7 and -1.2 respectively. It is evident from the figure that the observed ISD can be used to constrain the slope of the luminosity function, if the statistical error bars could be reduced. We have noted that the magnification bias factor in the biased lens cross-section is calculated for point sources. However, this may not be true for the sources of the lensed arcs, and their magnification bias could be negligible (e.g. [37]). Therefore, we have calculated the ISD assuming no bias. The long dashed curve in the right panel of Figure 3 shows the ISD without the bias. For all predictions, we have assumed $z_s=2$ for the source redshift. We have checked the effect of adopting different source redshifts $z_s=1.5$ and $z_s=3.0$ on the predicted ISD. The predicted $\mathrm{d}P_{\rm lens}/\mathrm{d}\theta$ is not affected, because the corresponding increase (decrease) in $P(>\theta_{\rm cut})$ almost perfectly cancels out the increase (decrease) in $\mathrm{d}P/\mathrm{d}\theta$. This implies that the expected ISD would not be drastically different had we accounted for the distribution of source redshifts instead of assuming a single value for the source redshift.

4. Summary

We have presented the SARCS sample from the completed CFHTLS-WIDE and CFHTLS-DEEP, covering a combined unmasked area of $\sim$150 deg^2 in the sky. The lens sample is compiled through a semi-automatic technique consisting of using ARCFINDER algorithm, followed by visual inspection and ranking of the candidates. We have compiled a total of 127 candidates in the SARCS sample. From the complete sample, 54 are promising lens systems.

We have measured the azimuthal distribution of (giant) arcs from the SARCS sample and found consistency with the predictions by the authors of [26]. However, the simulations used for the predictions need to be improved by implementing realistic physics, whereas larger samples with better understanding of the selection function will allow us to test different physical models of gas cooling, and feedback that are used as inputs in the simulations. The SARCS sample allowed, for the first time, to probe the intermediate mass regime corresponding to group-scale halos via the ISD. We have shown that the density profile of the halos is well-reproduced by a combined profile (NFW and Hernquist) at the group-scales, which is consistent with the predictions. We have found that varying the model parameters have degenerate effects on the ISD, however, if priors from independent methods are used on one of these relations, the observed ISD could be used to constrain, for example, the $c-M$ relation.

We have shown the possibility to use arcs statistics in constraining some of the scaling relations of the models tested here. However, the models may be simplistic and may need refinement as the lens samples become larger with upcoming surveys. On the observational side, understanding the selection effects will become crucial to constrain model parameters with better accuracy. We hope to address some of these important issues in future studies.

Acknowledgements
This work is based on observations obtained with MegaPrime/MegaCam, a joint project of CFHT and CEA/DAPNIA, at the Canada-France-Hawaii Telescope (CFHT), which is operated by the National Research Council (NRC) of Canada, the Institut National des Science de l'Univers of the Centre National de la Recherche Scientifique (CNRS) of France, and the University of Hawaii. Also, this work is based in part on data products produced at TERAPIX and the Canadian Astronomy Data Centre as part of the Canada-France-Hawaii Telescope Legacy Survey, a collaborative project of NRC and CNRS.

References

[1] Blandford R D and Narayan R 1992 *Ann. Rev. A. & A.* **30** 311
[2] Kochanek C S 2006 *Saas-Fee Advanced Course 33: Gravitational Lensing: Strong, Weak and Micro*
[3] Swinbank A M, Webb T M, Richard J *et al* 2009 *MNRAS* **400** 1121
[4] Zitrin A and Broadhurst T 2009 *Ap. J. Lett.* **703** L132
[5] More A, McKean J P, More S *et al* 2009 *MNRAS* **394** 174
[6] Vegetti S, Czoske O and Koopmans L V E 2010 *MNRAS* **407** 225
[7] Suyu S H *et al* 2010 *Ap. J.* **711** 201
[8] Ferreras I, Saha P, Leier D, Courbin F and Falco E E 2010 *MNRAS* **409** L30
[9] Treu T and Koopmans L V E 2002 *Ap. J.* **575** 87
[10] Koopmans L V E, Treu T, Bolton A S, Burles S and Moustakas L A 2006 *Ap. J.* **649** 599
[11] More A, McKean J P, Muxlow *et al* 2008 *MNRAS* **384** 1701
[12] Myers S T *et al* 2003 *MNRAS* **341** 1
[13] Bolton A S, Burles S, Koopmans L V E, Treu T and Moustakas L A 2006 *Ap. J.* **638** 703
[14] Luppino G A, Gioia I M, Hammer F, Le Fèvre O and Annis J A 1999 *A. & A. Supp. Ser.* **136** 117
[15] Ebeling H, Edge A C and Henry J P 2001 *Ap. J.* **553** 668
[16] Zaritsky D and Gonzalez A H 2003 *Ap. J.* **584** 691
[17] Gladders M D, Hoekstra H, Yee H K C, Hall P B and Barrientos L F 2003 *Ap. J.* **593** 48
[18] Parker L C, Hudson M J, Carlberg R G and Hoekstra H 2005 *Ap. J.* **634** 806
[19] Krusch E, Rosenbaum D, Dettmar R J *et al* 2006 *A. & A.* **459** 759
[20] Mandelbaum R, Seljak U and Hirata C M 2008 *JCAP* **8** 6
[21] Balogh M L *et al* 2009 *MNRAS* **398** 754
[22] Rines K and Diaferio A 2010 *Astron. J.* **139** 580
[23] Cabanac R A *et al* 2007 *A. & A.* **461** 813
[24] More A, Cabanac R, More S *et al* 2012 *Ap. J.* **749** 38
[25] Hattori M, Kneib J and Makino N 1999 *Prog. Theor. Phys. Supp.* **133** 1
[26] Dalal N, Holder G and Hennawi J F 2004 *Ap. J.* **609** 50
[27] Bertin E and Arnouts S 1996 *A. & A. Supp. Ser.* **117** 393
[28] Oguri M 2006 *MNRAS* **367** 1241
[29] Keeton C R, Christlein D and Zabludoff A I 2000 *Ap. J.* **545** 129
[30] Zitrin A, Broadhurst T, Barkana R, Rephaeli Y and Benítez N 2011 *MNRAS* **410** 1939
[31] Hernquist L 1990 *Ap. J.* **356** 359
[32] Gnedin O Y, Kravtsov A V, Klypin A A and Nagai D 2004 *Ap. J.* **616** 16
[33] Macciò *et al* 2007 *MNRAS* **378** 55
[34] Bullock J S *et al* 2001 *MNRAS* **321** 559
[35] Yang X, Mo H J and van den Bosch F C 2008 *Ap. J.* **676** 248
[36] Vale A and Ostriker J P 2004 *MNRAS* **353** 189
[37] Narayan R and Wallington S 1993 *Liege Int. Ap. Coll.* **31** 217